

RESEARCH

Open Access



# Structural Performance Assessment of Derailment Containment Provision for Railway using a Grid Steel Frame

Tae-Hoon Kim<sup>1\*</sup> , Yun-Suk Kang<sup>1</sup> and Choon-Seok Bang<sup>1</sup>

## Abstract

The structural performance of derailment containment provision (DCP) was investigated using a grid steel frame. The DCP which was installed within the gauge of a track was capable of resisting the impact loading in the case of derailed wheels. It was also possible to control the excessive lateral movement of the derailed train. In this study, the structural performance of DCP with a post-installed anchor to a railway concrete sleeper was evaluated. For this purpose, a total of nine specimens were manufactured and static tests were conducted to investigate the structural performance. Furthermore, the shear resistance of the connecting anchor was also evaluated using grid steel frame specimens. The initial test indicated that the developed DCP for railway using grid steel frames had sufficient load-carrying capacity and performance equivalent to about 150% of the design load. The developed DCP also demonstrated sufficient load-carrying capacity up to about 140% of the designed load in combination tests that simulated conceivable boundary conditions. As analytical results, the overall DCP behavior for the specimen railway that utilized grid steel frames was appropriately tracked, and detailed information was presented.

**Keywords** Structural performance, Derailment containment provision, Derailed wheel, Grid steel frame, Shear resistance

## 1 Introduction

Since about 30 years ago, research on roads has been actively conducted to better understand the collision behaviors between cars and protection facilities, and to develop assessment methods for the design of vehicle protection facilities. However, the design concept for railroad car protection facilities has not been established. There is limited research on this subject, and there is no standard for assessing the performance of protection facilities against derailed trains.

Train derailments and collisions are disasters that occur infrequently but cause significant damage. However, accidents caused by train derailments are more common in nations with advanced railway technology, such as Europe, the United States, Canada, Japan, China, and South Korea (Ebrahimi et al., 2021; Wu et al., 2014, 2016).

From 2012 to 2016, a total of 33 railway accidents occurred in South Korea. Derailment accidents have accounted for 78.8% of these incidents in a total of 26 cases which suggests that they occur more often than other types of accidents. Derailment accidents can be fatal, and it is impossible to avoid them entirely owing to ineluctable factors such as human error and natural disasters. As a result, relevant technologies must be developed to reduce the potential damage and injury caused by derailed trains (Bae et al., 2020).

Journal information: ISSN 1976-0485 / eISSN 2234-1315.

\*Correspondence:

Tae-Hoon Kim  
thkim@krri.re.kr

<sup>1</sup> Advanced Railroad Civil Engineering Division, Korea Railroad Research Institute, 176, Cheoldobangmulgwan-Ro, Uiwang-Si 16105, Gyeonggi-Do, Korea

Derailment and collision tests on actual large-sized railroad vehicles have recently been conducted in South Korea to minimize the secondary damage caused by derailment by restraining or controlling derailed trains inside a designated area. However, a standard has not been defined for collision tests involving railway vehicles and structures. Thus, the impact load is determined in the design of the protection facilities by referring to the standards for vehicle collision tests of road safety facilities (Kim et al., 2018, 2019).

When a train derails, the vehicles and track structure are primarily damaged, and significant secondary damage occurs, such as the collision of the derailed train with an overbridge or high embankment (Lai et al., 2022; Zhu et al., 2020). Given that this damage is caused by the train's excessive lateral deviation, secondary damage may

be reduced if the lateral behavior is minimized after the train derails. Countermeasures are, therefore, required to limit the damage caused by derailed trains.

In Europe, three types of derailment containment provisions (DCPs) have been applied to minimize the spread of damage after a train derailment (see Fig. 1). Type 1 is a DCP installed inside the track gauge to collide with the derailed wheel, similar to Korean guardrail for derailment prevention. Type 2 is a DCP installed outside the track gauge to collide with the derailed wheel, and type 3 is a DCP installed outside the track gauge to collide with the axles and bogies of derailed trains (Booz Allen Hamilton, 2004). However, the standards for the design load, installation location, and specification are not well-established or well-systematized. There is a lack of validated data that can prove

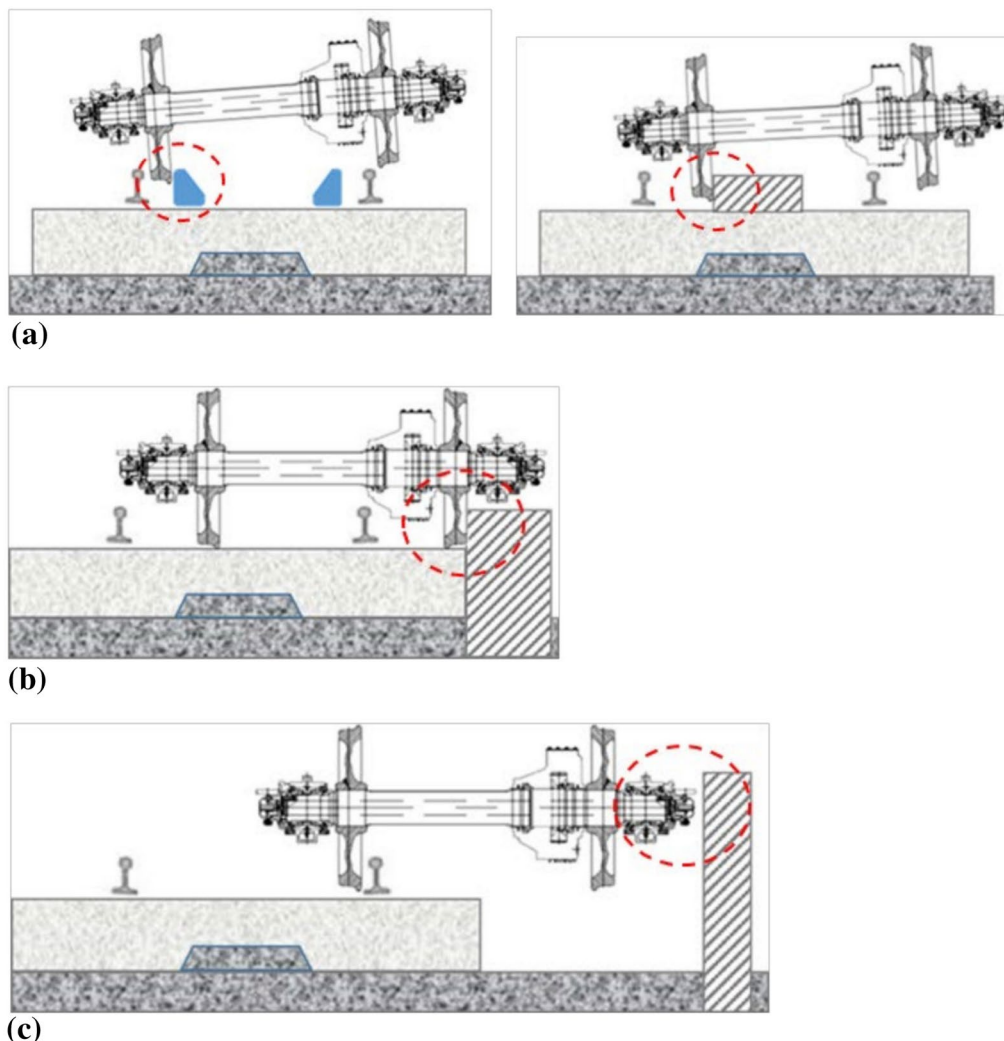


**Fig. 1** Concept of derailment containment provisions (Bae et al., 2020): **a** Type 1 (Collision at wheel level), **b** Type 2 (Collision at wheel level) and **c** Type 3 (Collision at bogie level)

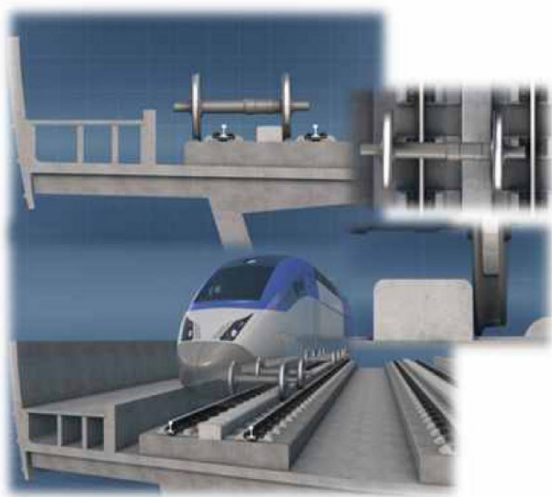


**Fig. 2** DCP(Derailment Containment Provision) conceptual diagram (Kim et al., 2018)

the effectiveness and economic feasibility of the analysis of the behavioral characteristics of derailed trains and the application of protection facilities (Bae et al., 2018; Brabie, 2007; Guo et al., 2016; Lai et al., 2021; Song et al., 2019).

Fig. 2 shows a newly developed DCP structure that uses wheel control to prevent lateral deviation of derailed trains (Cheon et al., 2019; Kim et al., 2018). When a train derails, the wheels are caught by the DCP located in the center of track, steered longitudinally along the DCP to prevent excessive lateral deviation of the train. Decreasing the lateral movement distance minimizes the impact energy that acts on the structure. This ensures efficiency and economic feasibility in the case of a single track since it can be constructed in a single structure, unlike the protection wall method that must be installed on both sides of the track gauge.

The developed DCP is a compacted plinth DCP type 1 structure that can improve protection performance in the event of derailment at 300 km/h for a high-speed railway with a curve radius  $R=3500$  m. It can resist up to 114 kN and 165.6 kN of derailment impact loads on straight and curved lines, respectively, and an impact energy of 3.3 kJ. Furthermore, the developed DCP is a railway protection system that can facilitate high-quality rapid construction and derailment recovery within the track blocking time (3 h at night) as a rapid construction structure on operating lines. Based on previous studies, the load was calculated using the acceleration data for a mass. To compare and evaluate this result with the load cell, a drop test in which other influencing factors were excluded was performed, as shown in Fig. 3 (Kim et al., 2019, 2020).



**Fig. 3** Drop weight test (Kim et al., 2019, 2020)

## 2 DCP for Railway Using a Grid Steel Frame

This study proposed the development of DCP that can be constantly fastened across the sleeper and the top surface of the sleeper in the form of a grid steel frame to control excessive deviation of a derailed train on a railroad track, as illustrated in Fig. 4.

The proposed construction method can prevent the wheels from derailing owing to lateral pressure while facilitating simple installation and removal of the lateral pressing device in the process of fixing and installing the grid steel frame on the railroad track using a fixture that includes an anchor bolt on the top surface of the sleeper. This threading process with chemical anchor is designed and validated to ensure that there is no damage to the structural capacity and integrity of the original sleepers.

As such, as shown in Fig. 4, the transverse frames are connected to the inner surfaces of both longitudinal frames to form a lattice shape. They are installed in the inner space formed between the inner surfaces of both longitudinal frames of the grid steel frame and the grid steel frame in which fixing holes are formed at both ends and the middle portions of the two longitudinal frames, respectively. This also includes a lateral pressing device that allows a pressing operation to introduce a lateral force to the grid steel frame fixed to the sleeper in the working space above it.

It is possible to prevent excessive lateral deviation of a derailed train by utilizing the DCP and the developed grid steel frame. Furthermore, the DCP is more stable and easier to remove, making it more effective to maintain.

## 3 Initial Test

### 3.1 Experimental Investigation

The lateral pressing device used in the process of fastening and installing the grid steel frame utilized fixtures that included anchor bolts on the top surface of the sleeper that may be readily installed in the DCP for a railway using a grid steel frame. Furthermore, its structural

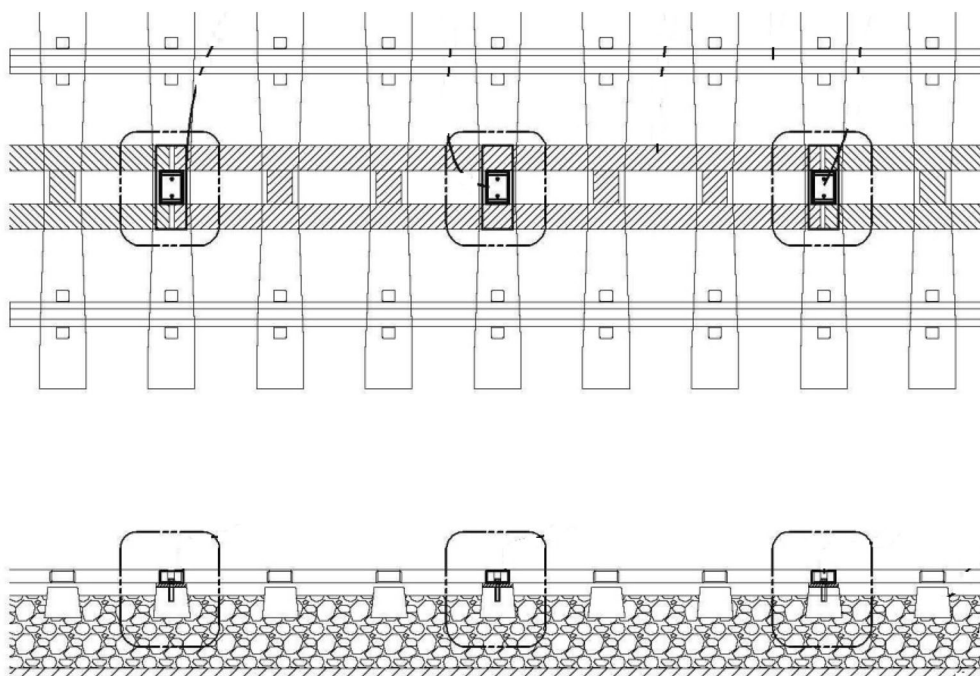


**Fig. 4** Proposed derailment containment provision for railway using a grid steel frame (Top view and side view)

type can also prevent train wheels from derailing via lateral pressurization.

It was critical to secure the connection between the sleeper and the grid steel frame in this type of structure. As a result, a static experiment was conducted to assess the structural integrity and load-carrying capacity of the DCP that was developed for the first time in Korea, and the grid steel frame coupling test body.

A full-scale partial test body, as illustrated in Fig. 5, was built to systematically assess the performance of DCP for railways using the grid steel frames. To simulate a full-scale test, the initial test specimen was fabricated as a full-size partial specimen without utilizing a scale model, and it had the same boundary conditions as the full-scale model. The specimen's design took into account practical constructability, and throughout the production process, the factors that were likely to cause construction errors were closely evaluated.

Three initial test specimens, S\_DCP-1, S\_DCP-2, and S\_DCP-3, were fabricated using the same specifications for comparison and verification. The design compressive strength of the concrete sleeper was 50 MPa, the modulus of elasticity of the grid steel frame and fixture steel was 210,000 MPa, and the yield strength of the grid steel frame and fixture steel was 355 MPa.

The impact load is conveyed to the sleeper via the anchor when a train derails and collides with a DCP.

The M20 anchor was chosen based on the DCP structural thickness and the potential penetration depth when utilizing the grid steel frame. The depth of penetration was determined to be 90 mm.

For the cross-section of the DCP, the height was set at 125 mm, the grid steel frame at 100 mm, the fixed base plate at 20 mm, and the insulating rubber pad at 5 mm based on preliminary analysis using the KTX vehicle.

The initial test specimen for evaluating the structural performance of the DCP for a railway utilizing a grid steel frame is depicted in Fig. 5. As indicated in Fig. 6, a static loading test was performed. During the experiment, a load plate was fabricated and utilized to test the specimen's stability. An experiment was conducted by fabricating a steel loading jig to replicate the load exerted by the wheels of a train in contact with the DCP during derailment. The jig was built with sufficient stiffness to prevent deformation owing to the load by adhering to the DCP without achieving yield under the designed load. To transmit a uniform load to the specimen via the jig, a 15 mm rubber was inserted between the jig and the specimen throughout the experiment. Furthermore, the center of gravity of the plate and the center of the actuator were aligned to reduce the influence of eccentricity. The lifting of the DCP can produce stress in the anchor in the vertical direction. Hence, the utilization of a carefully constructed bracket can reduce the lifting of the specimen and the consequent stress.

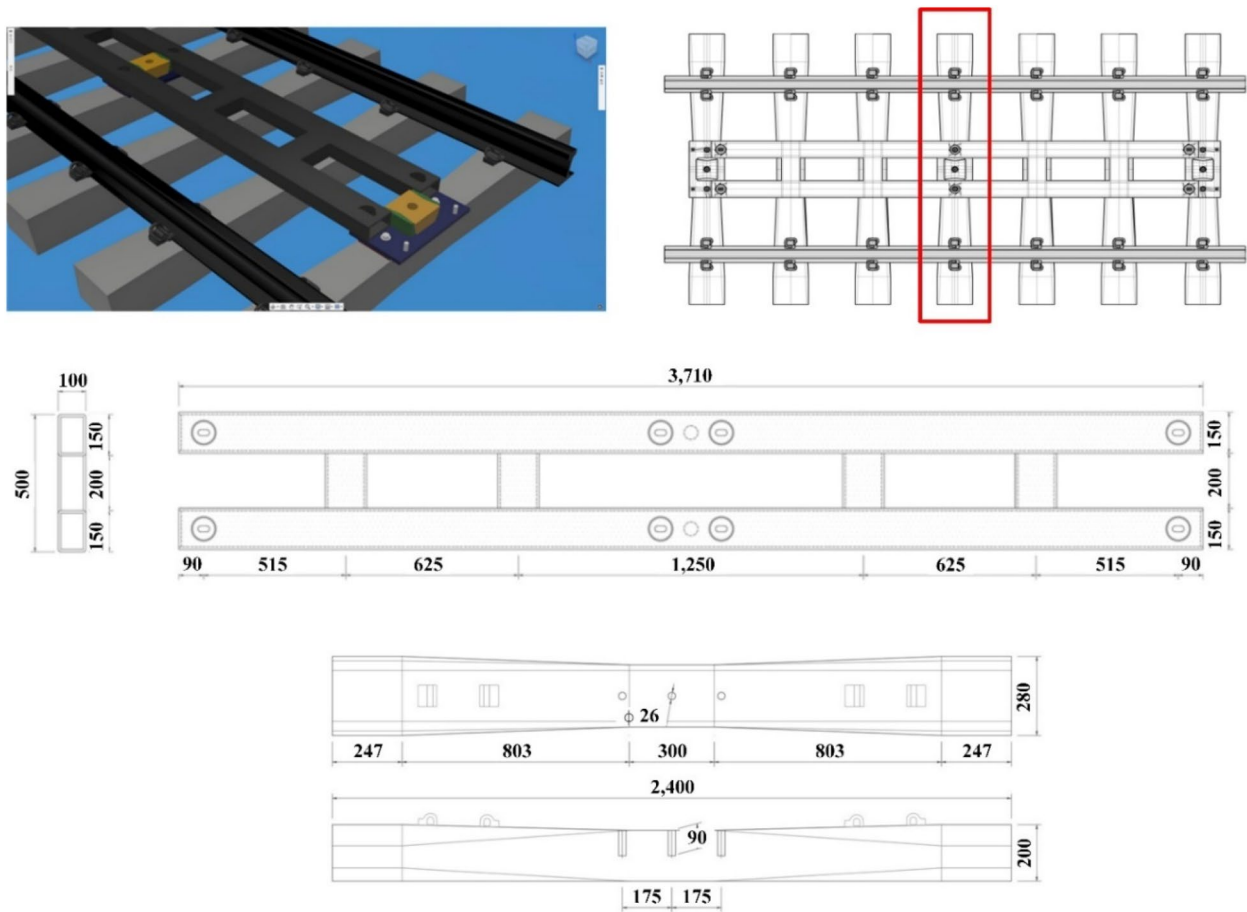


**Fig. 5** Element level specimens for derailment containment provision (Top view, dimensions in mm)



**Fig. 6** Loading set-up for element-level specimens

A 500 kN actuator with a maximum stroke of 250 mm was used for the loading test. The displacement control was applied at the same pace that speed was 1 mm/min. As shown in Fig. 7, the load–strain relationship was generated based on the measured load–displacement relationship, and a strain gauge (S1-B, S2-B) and LVDT (L1-B\_H, L2-B\_H) were mounted to the specimen. The maximum load and displacement delivered to the

original test specimen were measured when a static load was applied until the DCP failed. Furthermore, crack propagation was analyzed according to the loading stage to determine the failure mechanism of each specimen.

The load–displacement curves for the initial test specimen are shown in Fig. 8a and b. The experimental value of S\_DCP-1 was 238.3 kN, which demonstrated sufficient load-carrying capacity up to 144% of the

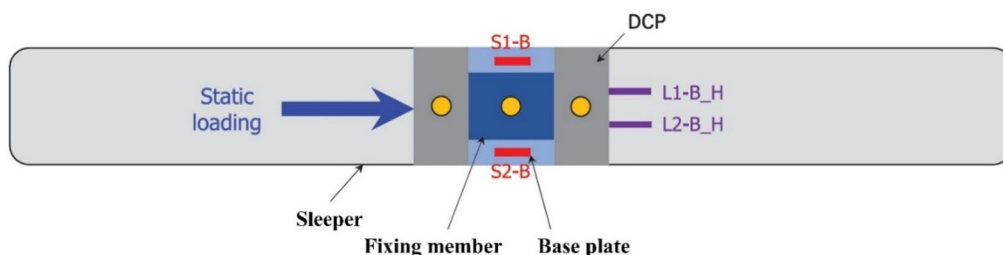


**Fig. 7** Experimental setup used for element-level specimens (Top view)

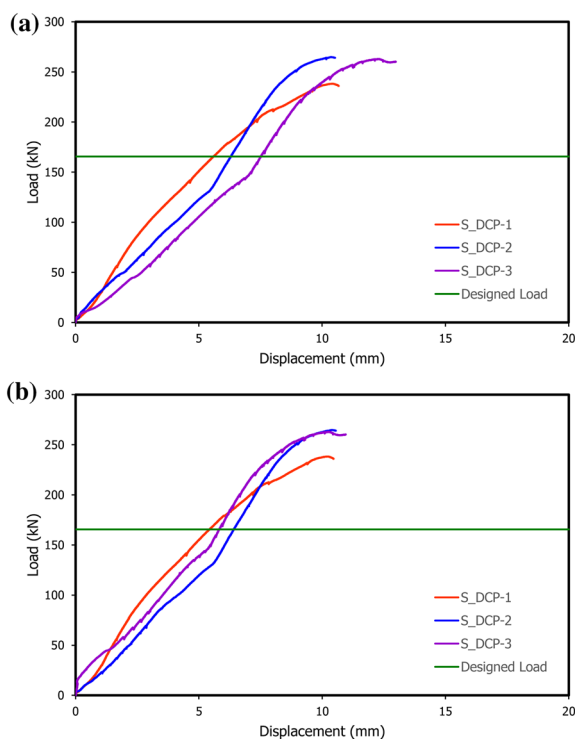


**Fig. 8** Lateral load–lateral displacement relationship for element-level specimens: **a** L1-B\_H and **b** L2-B\_H



**Fig. 9** Damage for element level specimen S\_DCP-2

connecting anchor. According to this damage pattern, strong shear stress acts on the anchor in a direction perpendicular to the edge of the DCP concrete owing to wheel collision. Therefore, the anchor should be carefully designed and constructed.

Steel failure, concrete failure, and concrete pryout failure are the three types of failures experienced by anchors subjected to a shear force (ACI Committee318, 2014; KCI, 2017). When a shear force acts on the anchor in a direction perpendicular to the edge of the concrete, as in this experiment, it is susceptible to concrete failure rather than anchor failure, as observed in Fig. 9. Even for this result, the SD400 anchor did not fail under the ultimate load condition, and the strength reduced after the maximum load was reached owing to brittle concrete end failure. Furthermore, with a shear load, concrete failure occurred before anchor failure. Based on these findings, sufficient resistance performance of the anchor grout in addition to an appropriate anchor design is required to achieve ductile behavior when the train wheel collides with the DCP during derailment.

designed load of 165.6 kN. The experimental value of S\_DCP-2 was 264.9 kN, which demonstrated sufficient load-carrying capacity up to 160% of the designed load of 165.6 kN. Furthermore, the experimental value of S\_DCP-3 was 263.0 kN, thus, the load-carrying capacity was up to 159% of the designed load of 165.6 kN.

Fig. 9 shows the typical crack pattern for the S\_DCP-2 specimen at the ultimate load condition. Cracks appeared along the edge of the concrete end of the tension section where the bending moment of the DCP anchor fixture was generated when the maximum load-carrying capacity was attained. Subsequently, as the applied load was increased, an increase in the displacement was observed owing to the yielding of the

### 3.2 Analytical Investigation

In this study, RCAHEST (Reinforced Concrete Analysis in Higher Evaluation System Technology) (Kim et al, 2003, 2005), a previously developed nonlinear finite element analysis program, was modified and utilized to forecast the behavioral characteristics of DCP for railways using grid steel frames.

RCAHEST was created by the authors and other researchers by including the RC plane stress element, interface element, and PS steel element into the finite element analysis program, FEAP ver. 7.2 (Taylor, 2000), developed by Taylor at the University of California, Berkeley.

In this study, a previously evaluated nonlinear material model for reinforced concrete was used. This process is summarized below.

First, the crack model was limited to generating a second crack orthogonal to the first crack using a non-orthogonal fixed crack model, thereby compensating for the limitation of the orthogonal fixed crack model, which underestimates the concrete stiffness. Furthermore, by inducing cracks to form at right angles to the direction of the actual principal stress, the stiffness of the concrete was accurately predicted.

The fundamental elastoplastic failure model described the material model of the concrete prior to cracking. After cracking, nonlinearity is apparent in the biaxial stress state. As illustrated in Fig. 10, the tensile stiffening model examines the tensile stress load of concrete in the direction perpendicular to the crack based on the orthotropy of the material nonlinearity of the reinforced concrete element after cracking. The compressive stiffness model in the crack direction considers the reduction in the compressive stiffness of the concrete. Furthermore, the transmission model at the crack surface considers the shear transmission effect of the concrete.

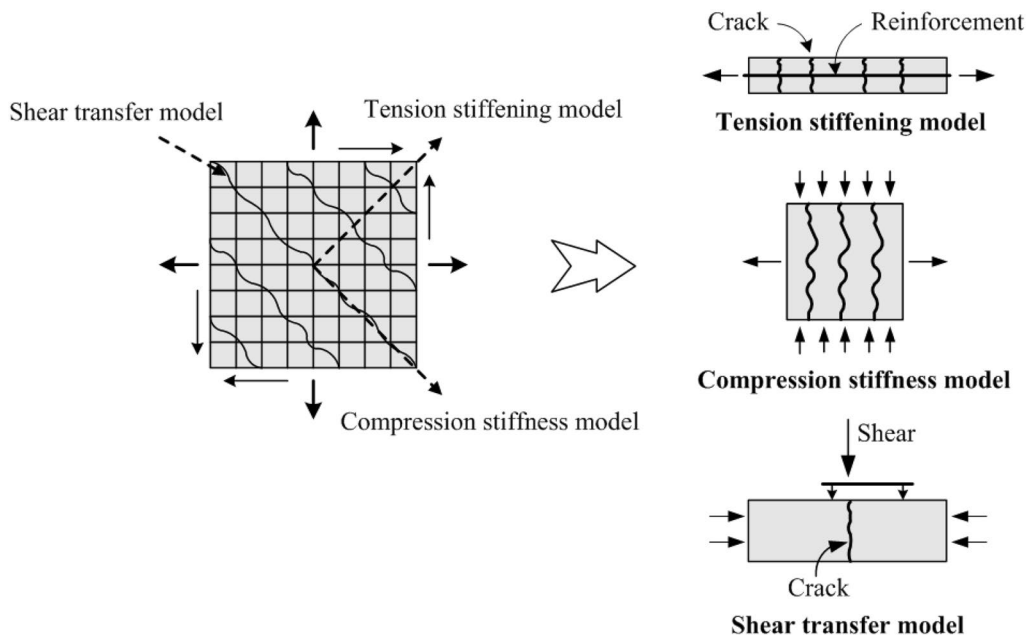
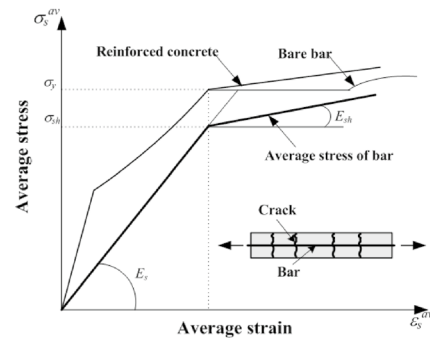


**Fig. 10** Cracked concrete model

The reinforcing bar material model simulated the behavior features after the yielding of the reinforcing bar embedded in the concrete by considering the characteristics of only the bar as well as the effect of attachment to the concrete. There was no stress increase owing to the yielding of the reinforcing bar in the cracked region in Fig. 11. However, given that the average stress increases as the stress of the internal reinforcing bar increases, the yield plateau phenomenon of the reinforcing bar’s stress–strain relationship is not manifested. A bilinear model



$\sigma_s^{av}$  = average steel stress;  $\sigma_y$  = yield strength of bar;  
 $\sigma_{sh}$  = offset stress point for the initiation of strain hardening of the bar;  
 $E_s$  = initial bar stiffness;  $E_{sh}$  = strain hardening rates of the bar embedded in concrete;  
 $\epsilon_s^{av}$  = average steel strain

**Fig. 11** Reinforcing bar model in concrete

could be employed to track the behavioral characteristics of such reinforcing bars after yielding, and this has been verified by the authors and others (Kim et al., 2003).

For finite element analysis of the initial specimens of DCP for railway using grid steel frames, the specimens were divided into a total of 35 elements, including 28 RC plane stress elements, 6 elastoplastic plane stress elements, and 1 interface element, as shown in Fig. 12. A 3-point Gaussian integration was applied to the RC plane stress element as an isoparametric element with 8 nodes. In addition, the interface element was an isoparametric element with 6 nodes. The interface elements between the sleeper and the DCP enhance the modeling of the effects of the slip and the local compression. The interface model for the boundary plane with different sections is based on the discrete crack concept, which uses the relationship between the stress and the localized deformations. The model is one dimensional and has no thickness; the relations of normal force versus the normal displacement and the shear force versus the shear displacement are described.

Fig. 13 shows a typical example of the aforementioned analysis results. The results for S\_DCP-2 are for an ultimate load of 252.6 kN, which is approximately 5% less than the experimental value of 264.9 kN. The failure mode of DCP for railways that use grid steel frames was reliably tracked. The stress cloud diagram of the finite element calculation to analyze the force of the entity after loading in more detail, as shown in Fig. 14. A comparison with the experimental data indicated that the applied nonlinear finite element analysis program RCAST accurately tracked the DCP's behavioral characteristics.

#### 4 Combination Test

##### 4.1 Experimental Investigation

In the initial test in the preceding section, a full-scale partial specimen was designed and fabricated to assess the performance of the DCP, and a static loading test was performed by accurately modeling the boundary conditions. The designed DCP demonstrated adequate load-carrying capacity in comparison to the designed load based on the relevant tests and analyses. It was

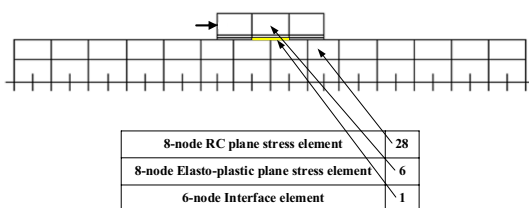


Fig. 12 Finite element mesh for element-level specimens

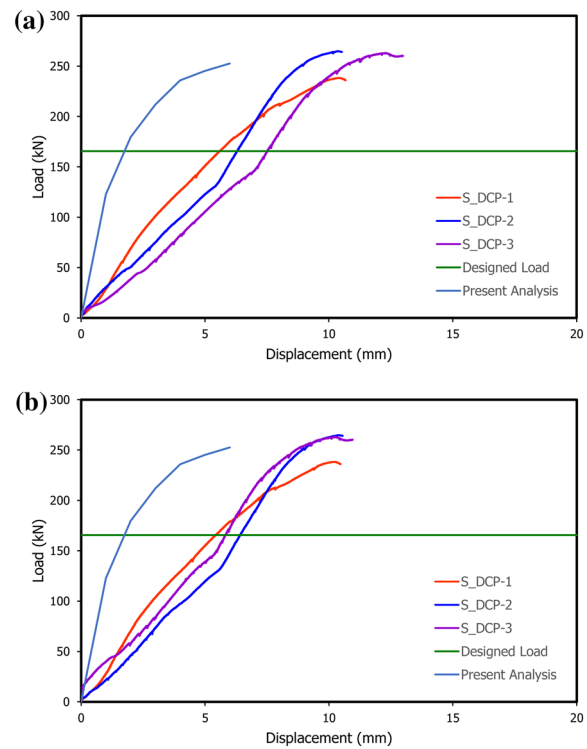


Fig. 13 Sample of comparison of analytical and experimental results: a L1-B\_H and b L2-B\_H

demonstrated that when a train wheel collides with a DCP as a result of derailment, ductile behavior is exhibited.

In this section, full-scale combination specimens were designed as shown in Fig. 15. Two combination specimens were fabricated, each with the real boundary conditions. The objective was to review the structural performance of the DCP and sleeper, the shear performance of the anchor, and the structural performance of the DCP connection. As shown in Fig. 16, there are three cases: Case-1 applies the load between the anchor

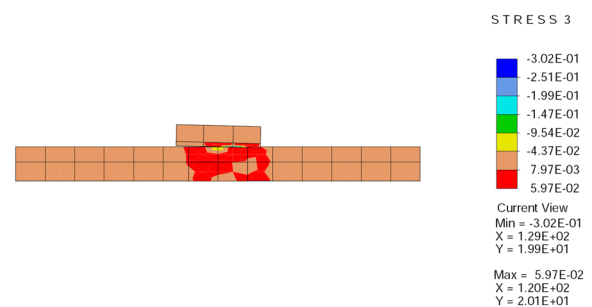
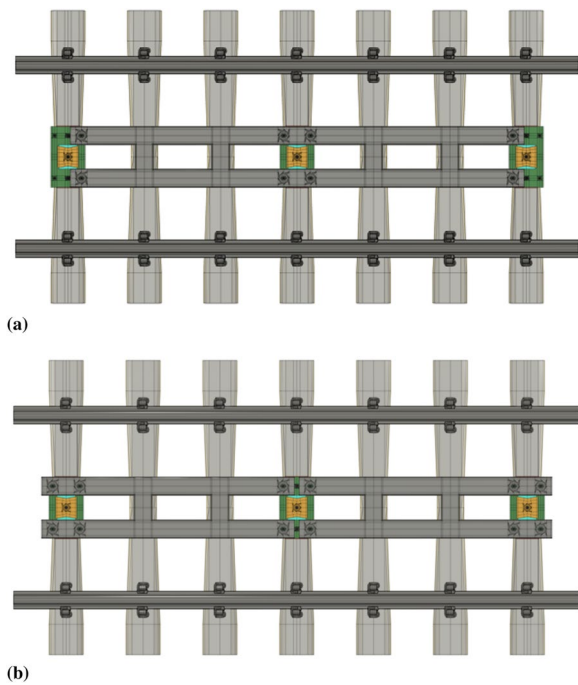


Fig. 14 Sample of stress cloud diagram of the finite element calculations for element-level specimens



**Fig. 15** Structure level specimens for derailment containment provision (Top view): **a** Case-1, 2 and **b** Case-3

points, Case-2 applies the load to the center of the DCP, and Case-3 applies the load between the points.

In this case, the designed compressive strength of the concrete sleeper was set to 50 MPa, the modulus of elasticity of the grid steel frame and fixture steel was set to 210,000 MPa, and the yield strength of the grid steel frame and fixture steel was set to 355 MPa. The anchor of the DCP combination specimen for a grid steel frame was selected as an M20 anchor considering the DCP structure thickness and the potential penetration depth. The penetration depth was determined to be 90 mm. Furthermore, the DCP height was set at 125 mm based on a preliminary analysis of the KTX vehicle. The grid steel frame was set to 100 mm, the fixed base plate was set to 20 mm, and the insulating rubber pad was 5 mm thick, which are the same values as that of the initial test specimen.

Failure tests with the load combinations shown in Figs. 16 and 17 were performed to evaluate structural performance in the DCP combination specimens. The load exerted by the train’s wheels in contact with the DCP during derailment was simulated. The loading plate was produced with sufficient stiffness to adhere to the DCP under the designed load without flexing, as in the initial test. For consistent load transmission, experiments were conducted using 15 mm rubber components inserted between the jig and the specimen. Furthermore, since the elevation of the DCP can cause stress in the anchor in the vertical direction, this was minimized by utilizing

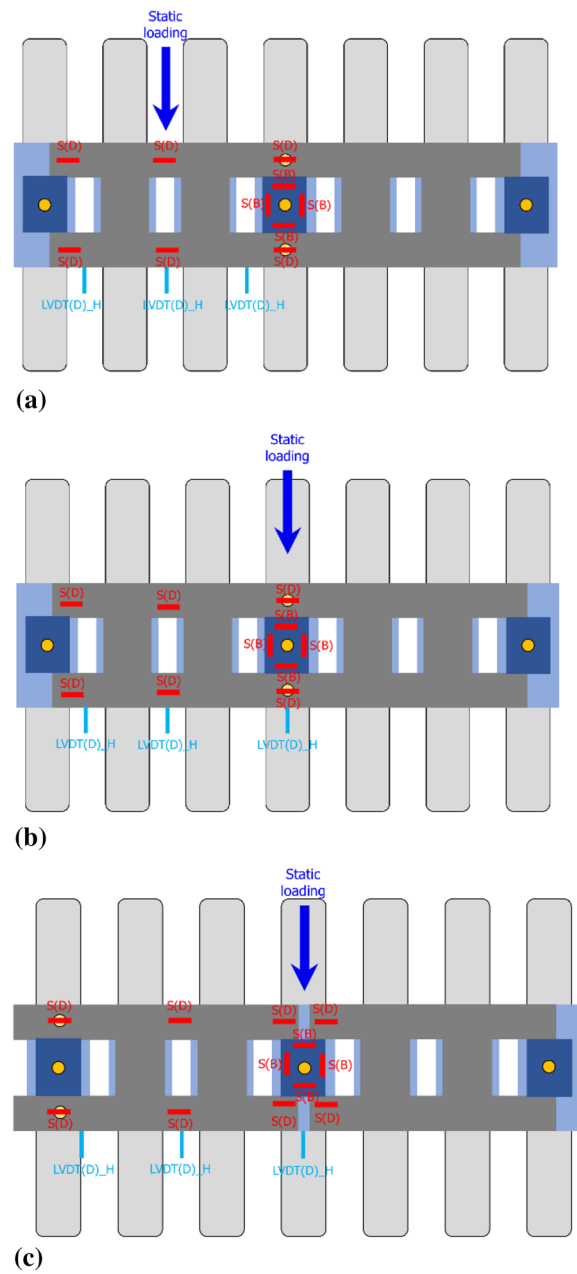


**Fig. 16** Overview of the structure level specimens (Top view): **a** Case-1, **b** Case-2 and **c** Case-3

a specially constructed bracket. The centroid of the plate and the center of the actuator were aligned to reduce the influence of eccentricity.

The actuator had a capacity of 500 kN and a maximum stroke of 250 mm. The loading speed was set to 1 mm/min, and the displacement was set such that it did not impact the specimen. The load–displacement relationship was determined based on the static tests for three load conditions. A strain gauge and LVDT

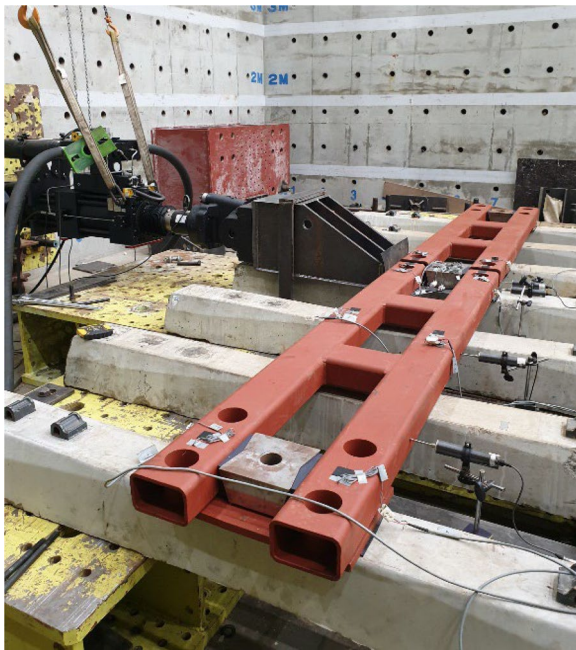


**Fig. 17** Loading set-up for structure-level specimens (Case-3)

were attached to the specimen as illustrated in Fig. 16. When the DCP failed under the application of a static load, the ultimate load and displacement were measured, and the failure mode of each combination specimen was identified by examining the crack propagation according to the loading stage.

Fig. 18 shows the load–displacement curve for DCP for the railway combination specimen using a grid steel frame. It was obvious that the pinching effect is caused by the bond slips between the DCP and the base plate with rubber pad.

The experimental value for Case-1\_1 was 210.5 kN, and sufficient load-carrying capacity was observed up to 127% of the designed load of 165.6 kN. The experimental value for Case-1\_2 was 290.2 kN, and sufficient load-carrying capacity was observed up to 175% of the designed load of 165.6 kN. In Case-2\_1, the experimental value was 210.4 kN, and sufficient load-carrying capacity was observed up to 127% of the designed load of 165.6 kN. The experimental value for Case-2\_2 was 209.8 kN, and sufficient load-carrying capacity was observed up to 127% of the designed load of 165.6 kN. The experimental value for Case-3\_1 was 210.4 kN, and sufficient load-carrying capacity was observed up to 127% of the designed load of 165.6 kN. Finally, the experimental value for Case-3\_2 was 250.5 kN, and sufficient load-carrying capacity was observed up to 151% of the designed load of 165.6 kN.

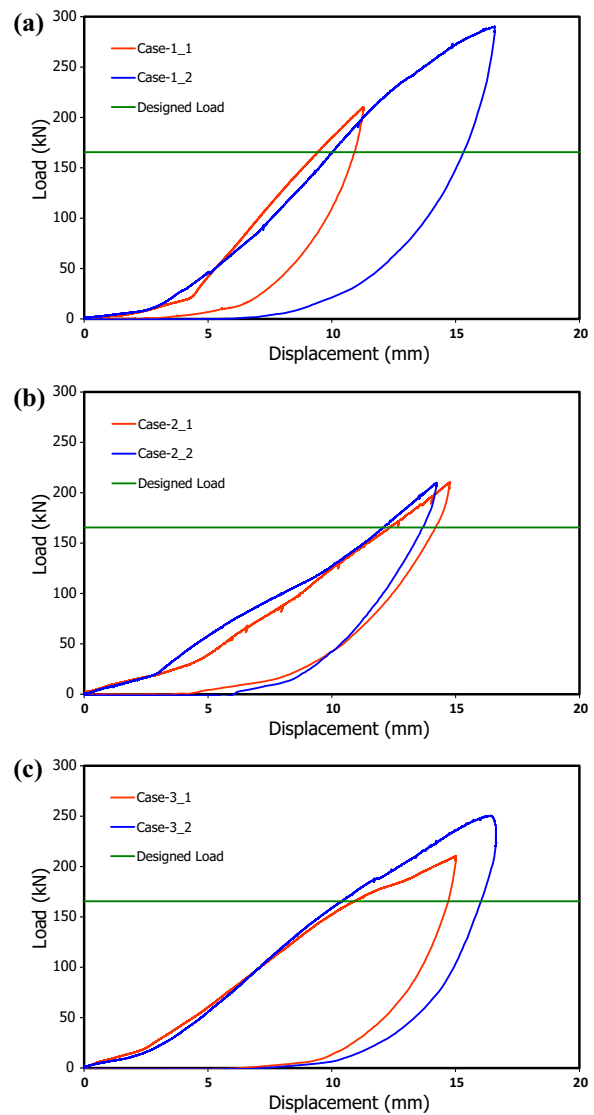


**Fig. 18** Lateral load–displacement relationship for structure level specimens: **a** Case-1, **b** Case-2 and **c** Case-3

The patterns of cracks developed under the ultimate load for typical specimens in Case-1, Case-2, and Case-3 are shown in Fig. 19. Cracks appeared along the edge of the concrete end of the tension section when the maximum load-carrying capacity was attained. Subsequently, an increase in the displacement was observed owing to the yielding of the connecting anchor. Based on the damage patterns of the combination specimens, it was determined that a considerable shear force acts on the anchor in a direction perpendicular to the edge of the DCP concrete owing to wheel contact. Therefore, the anchor should be carefully designed and constructed.

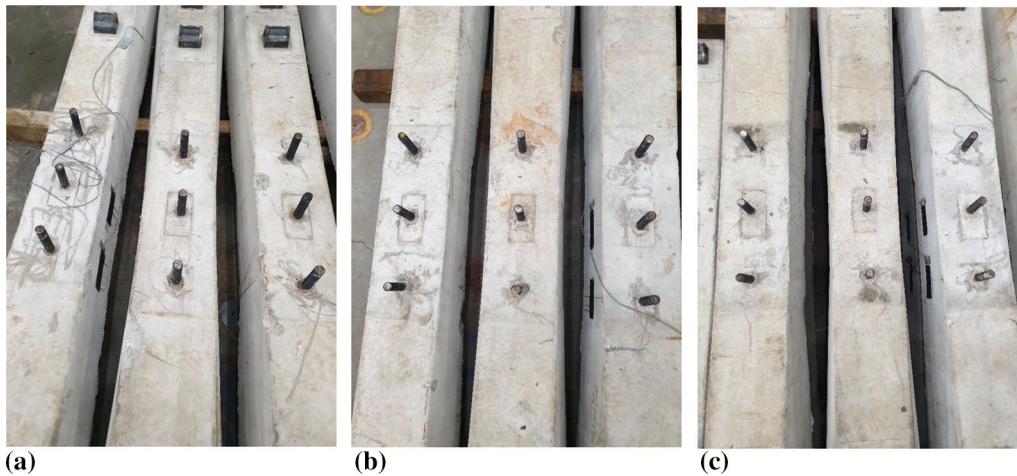


**Fig. 19** Damage for structure level specimens: **a** Case-1, **b** Case-2 and **c** Case-3

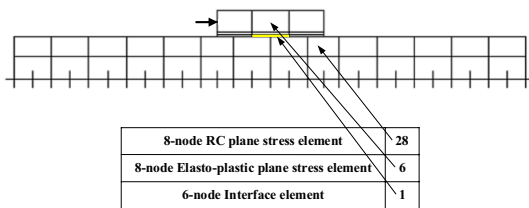


**Fig. 20** Finite element mesh for structure-level specimens

### 4.2 Analytical Investigation

The previously developed nonlinear finite element analysis program RCAHEST (Kim et al., 2003, 2005; Kim, 2022) was used to predict the behavioral characteristics of the combination specimen of DCP for railway using grid steel frames, as described in the previous section.

The DCP combination specimens were separated into 35 elements for finite element analysis, comprising 28 RC plane stress elements, 6 elastoplastic plane stress elements, and 1 interface element, as illustrated in Fig. 20. The RC plane stress element was an isoparametric element with 8 nodes, which was integrated using 3-point Gaussian integration. The interface element was an isoparametric element with 6 nodes.

Fig. 21 shows an example of the results of the aforementioned analysis. The analytical result for Case-2 is for an ultimate load of 202.1 kN, which is approximately 4% less than the experimental values for Case-2\_1 of 210.4 kN and Case-2\_2 of 209.8 kN. The failure mode of the combination specimen of DCP for railways that use grid steel frames was closely monitored. The stress cloud diagram of the finite element calculation to analyze the force of the entity after loading in more detail, as shown in Fig. 22. Compared to the actual data, it is clear that the utilized nonlinear finite element analysis program

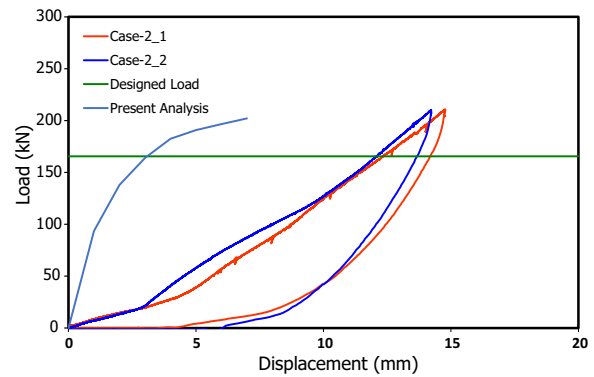


**Fig. 21** Sample of comparison of analytical and experimental results for structure level specimen Case-2

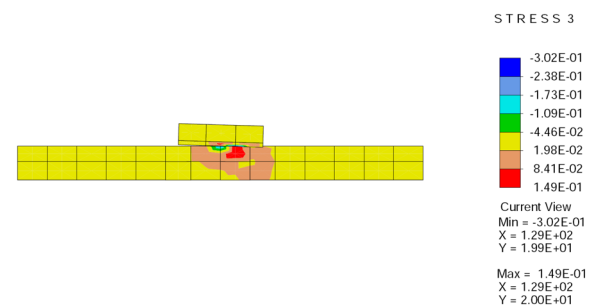


**Fig. 22** Sample of stress cloud diagram of the finite element calculations for structure-level specimens

RCAHEST accurately follows the overall behavioral characteristics of the DCP.

Further research is expected to allow for more accurate tracking of ductility ability, which shows a slight difference if the interface characteristics and nonlinear behavior properties of DCP for railways using grid steel frames,

such as fixed base plates and insulating rubber pads are precisely identified.

Based on a series of comparisons of experimental and analytical results, it was deduced that the nonlinear finite element analysis technique presented in this study to predict the behavioral characteristics of DCP can facilitate the identification of its overall behavioral characteristics and structural performance assessment. Furthermore, it is expected to replace the experimental performance assessment, which is hindered by time and cost constraints.

## 5 Conclusions

To minimize the excessive deviation of a derailed train on railroad tracks, a DCP in the shape of a grid steel frame was developed to be positioned over the sleeper and the top surface of the sleeper. The following conclusions were established after conducting experimental and analytical studies to evaluate structural performance.

- The structural performance of the DCP for railways using grid steel frames, which can prevent train wheels from derailing when subjected to lateral pressure, was evaluated based on experimental and analytical studies. The developed DCP could simplify the installation of the lateral pressing device in the process of fixing and installing the grid steel frame on the railroad track using fixtures, including anchor bolts on the upper surface of the sleeper. In addition, its economic feasibility and constructability were verified.
- The initial test indicated that the developed DCP for railway using grid steel frames had sufficient load-carrying capacity and performance equivalent to 144%, 160%, and 159% of the design load.
- The developed DCP demonstrated sufficient load-carrying capacity up to 127% and 175% (Case-1\_1 and Case-1\_2), 127% and 127% (Case-2\_1 and Case-2\_2), and 127% and 151% (Case-3\_1 and Case-3\_2) of the designed load in combination tests that simulated conceivable boundary conditions. Its validity was also confirmed.
- The analytical values for the maximum load in the initial and combination tests exhibited approximate deviations of 5% and 4% from the experimental values, respectively, because of the nonlinear finite element analysis used in this study. As a result, the overall DCP behavior for the specimen railway that utilized grid steel frames was appropriately tracked, and detailed information was presented. This allowed for the analytical evaluation of the structural performance, which could then be utilized for structural

performance assessment and design review of the DCP.

- Cracks appeared at the edge of the concrete end of the tensile section where the bending moment of the DCP anchor fixture occurred when the DCP reached its maximum load-carrying capacity. Subsequently, as the applied load was increased, an increase in the displacement was observed owing to the yielding of the connecting anchor. These damage patterns suggested that a high shear force was exerted on the anchor in a direction perpendicular to the edge of the DCP concrete owing to wheel impact.
- It is expected that if the interface characteristics and nonlinear behavior of DCP for railways using grid steel frames, such as the fixed base plate and insulating rubber pad are precisely identified in further studies, the ductility and other properties, which exhibit some differences based on nonlinear analysis, will be more accurately tracked.

## Acknowledgements

This research was supported by a grant (RS-2021-KA163289) from the Railway Technology Research Program, funded by the Ministry of Land, Infrastructure, and Transport of the Korean government.

## Author contributions

THK planned this paper, developed the finite element model, analyzed the experimental results and the numerical results. YSK analyzed the experimental results and the numerical results. CSB constructed the finite element model. All authors read and approved the final manuscript.

## Funding

This research was supported by a grant (RS-2021-KA163289) from the Railway Technology Research Program, funded by the Ministry of Land, Infrastructure, and Transport of the Korean government.

## Availability of data and materials

The research data used to support the finding of this study are described and included in the article. Furthermore, some of the data used in this study are also supported by providing references as described in the article.

## Declarations

### Competing interests

The author declares no competing interests.

Received: 11 January 2023 Accepted: 2 September 2023

Published online: 16 January 2024

## References

- ACI Committee 318 (2014). Building Code Requirements for Reinforced Concrete (ACI 318–14) and Commentary (ACI 318R–14). American Concrete Institute.
- Bae, H. U., Moon, J. H., Lim, S. J., Park, J. C., & Lim, N. H. (2020). Full-scale train derailment testing and analysis of post-derailment behavior of casting bogie. *Applied Sciences*, 10(1), 59.
- Bae, H. U., Yun, K. M., Moon, J., & Lim, N. H. (2018). Impact force evaluation of the derailment containment wall for high-speed train through a collision

- simulation. *Advances in Civil Engineering*. <https://doi.org/10.1155/2018/2626905>
- Booz Allen Hamilton (2004). Report on the findings of: Current practice and effectiveness of derailment containment provisions on high speed lines. HSL-Zuid Organisation, Issue 1, Ref: R00673.
- Brabie, D. (2007). Wheel-sleeper impact model in rail vehicles analysis. *Journal of System Design and Dynamics*, 1(3), 468–480.
- Cheon, H. S., Lim, S. J., Bae, H. U., Ryou, G. H., & Lim, N. H. (2019). Effects of the hump in concrete track on the post derailment behavior of freight car. *Journal of Korean Society for Urban Railway*, 7(2), 245–253. [in Korean].
- Ebrahimi, H., Sattari, F., Lefsrud, L., & Macchiotta, R. (2021). Analysis of train derailments and collisions to identify leading causes of loss incidents in rail transport of dangerous goods in Canada. *Journal of Loss Prevention in the Process Industries*, 72, 104517.
- Guo, L., Wang, K., Lin, J., Zhang, B., Chen, Z., Song, X., & Du, G. (2016). Study of the post-derailment safety measures on low-speed derailment tests. *Vehicle System Dynamics*, 54(7), 943–962.
- KCI (2017). KCI Model Code 2017. Korea Concrete Institute.
- Kim, J. H., Bae, H. U., Kim, J. W., Song, I. H., Lee, C. O., & Lim, N. H. (2018). Post-derailment behavior of casting bogie by full scale test. *Journal of the Korean Society for Railway*, 21(8), 815–829.
- Kim, N. H., Kang, Y. S., Bae, H. U., Kim, K. J., & Lim, N. H. (2020). Evaluation of impact resistance for derailment containment provision using drop weight test. *Journal of the Korean Society of Hazard Mitigation*, 20(5), 185–194.
- Kim, T.-H. (2022). Seismic performance assessment of deteriorated two-span reinforced concrete bridges. *International Journal of Concrete Structures and Materials*, 16(2), 123–135.
- Kim, T.-H., Cheon, J.-H., & Shin, H. M. (2012). Evaluation of behavior and strength of prestressed concrete deep beams using nonlinear analysis. *Computers & Concrete*, 9(1), 63–79.
- Kim, T.-H., Kim, Y.-J., Kang, H.-T., & Shin, H. M. (2007). Performance assessment of reinforced concrete bridge columns using a damage index. *Canadian Journal of Civil Engineering*, 34(7), 843–855.
- Kim, T.-H., Lee, K.-M., Chung, Y.-S., & Shin, H. M. (2005). Seismic damage assessment of reinforced concrete bridge columns. *Engineering Structures*, 27(4), 576–592.
- Kim, T.-H., Lee, K.-M., Yoon, C.-Y., & Shin, H. M. (2003). Inelastic behavior and ductility capacity of reinforced concrete bridge piers under earthquake. I: theory and formulation. *Journal of Structural Engineering*, 129(9), 1199–1207.
- Kim, Y. D., Lim, S. J., Bae, H. U., Kim, K. J., Lee, C. O., & Lim, N. H. (2019). Some thought on the estimating of the impact force by an experiment. *Journal of Korean Society for Urban Railway*, 7(2), 205–213.
- Lai, J., Xu, J., Liao, T., Zheng, Z., Chen, R., & Wang, P. (2022). Investigation on train dynamic derailment in railway turnouts caused by track failure. *Engineering Failure Analysis*, 134, 106050.
- Lai, J., Xu, J., Wang, P., Chen, J., Fang, J., Ma, D., & Chen, R. (2021). Numerical investigation on the dynamic behaviour of derailed railway vehicles protected by guard rail. *International Journal of Vehicle Mechanics and Mobility*, 59(12), 1803–1824.
- Song, I. H., Kim, J. W., Koo, J. S., & Lim, N. H. (2019). Modeling and simulation of collision-causing derailment to design the derailment containment provision using a simplified vehicle model. *Applied Sciences*, 10(1), 118.
- Taylor RL. (2000). FEAP – A Finite Element Analysis Program Version 7.2 Users Manual, Volume 1 and Volume 2. University of California at Berkeley; CA, USA.
- Wu, X., Chi, M., & Gao, H. (2014). The study of post-derailment dynamic behavior of railway vehicle based on running tests. *Engineering Failure Analysis*, 44, 382–399.
- Wu, X., Chi, M., & Gao, H. (2016). Post-derailment dynamic behaviour of a high-speed train under earthquake excitations. *Engineering Failure Analysis*, 64, 97–110.
- Zhu, X., Lu, X.-Z., Cheng, Q.-L., & Li, Y. (2020). Simulation of the running attitude of a train after derailment. *International Journal of Crashworthiness*, 25(2), 213–219.

## Publisher's Note

Springer Nature remains neutral with regard to jurisdictional claims in published maps and institutional affiliations.

**Tae-Hoon Kim** Senior Researcher, Advanced Railroad Civil Engineering Division, Korea Railroad Research Institute, 176, Cheoldo-bangmulgwan-ro, Uiwang-si, Gyeonggi-do, 16105, Korea.

**Yun-Suk Kang** Chief Researcher, Advanced Railroad Civil Engineering Division, Korea Railroad Research Institute, 176, Cheoldobangmulgwan-ro, Uiwang-si, Gyeonggi-do, 16105, Korea.

**Choon-Seok Bang** Principal Researcher, Advanced Railroad Civil Engineering Division, Korea Railroad Research Institute, 176, Cheoldo-bangmulgwan-ro, Uiwang-si, Gyeonggi-do, 16105, Korea.

Submit your manuscript to a SpringerOpen® journal and benefit from:

- Convenient online submission
- Rigorous peer review
- Open access: articles freely available online
- High visibility within the field
- Retaining the copyright to your article

Submit your next manuscript at ► [springeropen.com](https://www.springeropen.com)